

Radiation induced Richtmyer-Meshkov instability: Numerical simulations and phenomenological analysis

Michel Legrand & Jean-Marie Clarisse

Commissariat à l’Energie Atomique, B.P. 12
91680 Bruyères le Chatel, France
michel.legrand@cea.fr
jean-marie.clarisse@cea.fr

Introduction

Laser induced Richtmyer-Meshkov (RM) instabilities have previously been described. In particular, the radiation induced shock in an ablator can generate a classical RM instability at the ablator/low density medium interface of a two layer target [1]. More recently a RM like instability has been described in the case of a corrugated ablation front [2, 3]: ablation pressure generates a rippled shock which induces a pressure perturbation that leads to an instability of the ablation front. In this work, we consider a thermal front propagating in a low opacity medium and encountering a high opacity medium. This generates an acceleration impulsion at the interface and a hydrodynamic instability which will be called here *radiation induced* RM instability.

Description of the system under consideration

The system, described in Figure 1, consists of a two layer target (CH foam/Al). The CH foam is irradiated by X-rays produced in a spherical Hohlraum by a typical LIL square impulse ($\Delta t = 3$ ns, rise time = 0.1 ns, $P_1 = 7.5$ TW). The resulting temperature time history in the hohlraum is given in Figure 2. The maximum Hohlraum temperature is of the order of 2 MK.

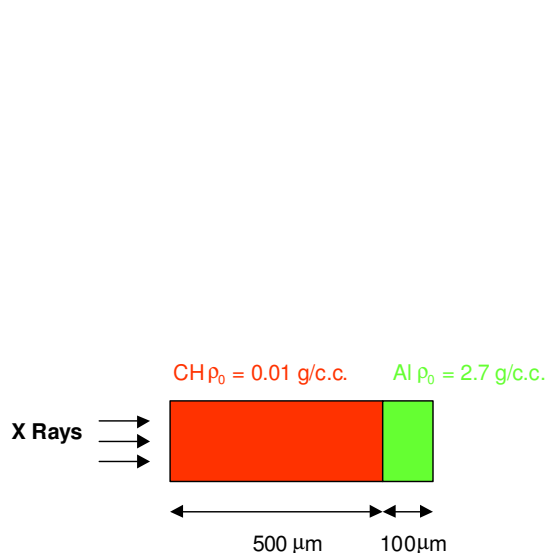


Figure 1: Two layer target layout.

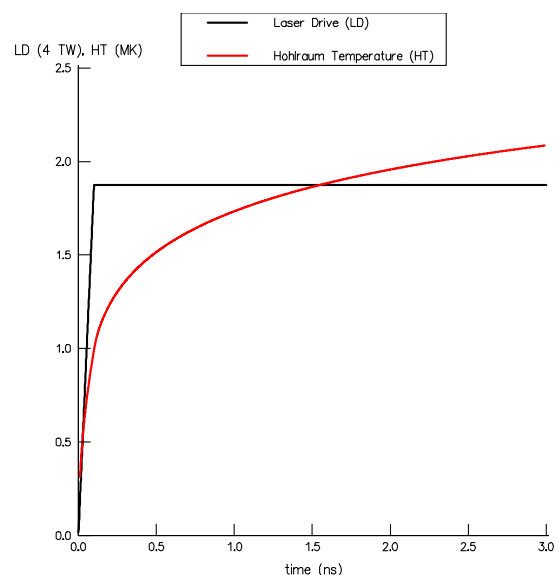


Figure 2: Laser power and temperature time histories.

Due to the incident X-ray flux, a supersonic thermal front propagates throughout the CH foam until it reaches the Al layer. This front entering an optically thicker material, the temperature on the Al side of the interface undergoes a sudden rise thus creating a pressure pulse which sets impulsively the interface into motion towards the lighter fluid (CH foam). Although this pressure jump tends to relax, the still rising Al temperature keeps on building an overpressure on the Al side leading to a sustained acceleration of the interface directed from the heavier to the lighter material. Soon the thermal front which keeps on propagating in the Al layer becomes subsonic, giving birth to an ablation flow in the deflagration regime. Such a scenario is obviously prone to trigger interfacial instabilities in the presence of initial surface defects. The fact that the interface is subject to an impulsive acceleration immediately suggests a possible acquaintance with the RM instability. However the details of the events at the origin of this impulsive motion differ drastically from the shock front-interface interaction of the RM instability case. For this reason we decided to rely exclusively on careful numerical simulations of single mode interface perturbations, in the linear approximation, in order to build up an understanding of the phenomena at play in the present case.

Simulation methods

Many numerical simulations have been carried out with FCI2, a 2D Lagrangian hydrodynamics code designed at CEA for inertial confinement fusion and laser-matter interaction studies. But the first results with multi-group diffusion were very confusing in terms of perturbation amplitude behaviors. For this reason we compared FCI2 results with SILEX [4] results. SILEX is a linear perturbation code, very well suited to such studies. However this code is limited to the Rosseland diffusion approximation and we had to resort to the same hypothesis in FCI2 simulations. Some of our difficulties were clearly related to simulation convergence problems. This led us to a careful FCI2 convergence study in terms of spatial step sizes (Δx , Δy), and of initial perturbation amplitudes.

FCI2 simulations

1- Impulsive model

The interface is driven by a thermal wave which generates first an acceleration impulsion and therefore a RM-like interface instability. The impulsion is followed by a slowly varying acceleration which leads to interface stabilization. In the RM instability case, the growth factor Gf of the instability has the following form (according to the impulsive model)

$$Gf = \frac{a}{a_0^*} = At^* k \Delta U t$$

where a_0^* is a corrected initial amplitude of the perturbation, a the amplitude at time t , A_t^* the Atwood number after interaction, k the wave number of the perturbation and ΔU the velocity jump. The Atwood number after interaction and the velocity jump are simply related to the pressure jump. In the radiation induced RM instability case, the drive is a temperature and not a pressure and there is no simple relation between this temperature, the Atwood number after interaction and the velocity jump. This is the reason why we studied the relation between the growth factor and the wavelength only. The results of four FCI2 simulations ($\lambda = 20, 40, 80, 160 \mu\text{m}$) are shown in Figures 3 and 4. At the very beginning of the instability Gf seems to be a linear function of t (see Figure 3) but Figure 4 shows that this is a very crude result.

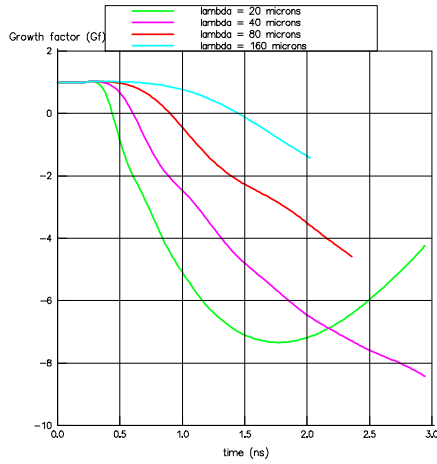


Figure 3: Growth factor of the instability (Gf).

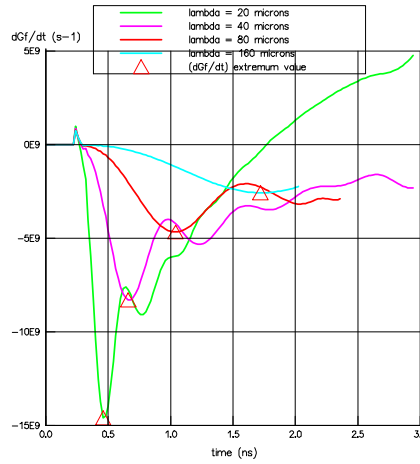


Figure 4: Growth factor time rate ($d(Gf)/dt$).

Later on, the growth factor begins to oscillate. A characteristic value of the growth factor time rate, $d(Gf)/dt$, is its extreme value $(d(Gf)/dt)_{ext}$ which is a quasi linear function of k (Figure5). This is a property of the impulsive model:

$$Gf = \frac{a}{a_0} = At^* k \Delta U t$$

which leads to $d(Gf)/dt = At^* \Delta U k$.

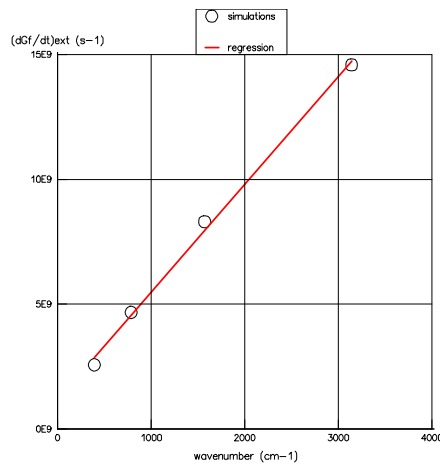


Figure 5: $(d(Gf)/dt)_{ext}$ as a function of the wavenumber.

Here we have: $(d(Gf)/dt)_{ext} = At^* \Delta U k$ and the slope observed in Figure 5 should be equal to $At^* \Delta U$. This would lead to $At^* = slope/\Delta U = 0.55$ which is very different from the Atwood number after interaction $At^+ = 0.25$ but which is much closer to $At_{1/2} = (At^- + At^+)/2 = 0.62$. This is probably related to the very short relative interaction time (interaction time/“observation” time) observed in RMI as compared to radiation induced RMI.

2- Beginning of the inversion phase

In radiation induced RMI, the acceleration is directed from the heavy medium to the light medium. In the pure RMI case, this situation leads to an inversion phase which begins right after the initial velocity jump. In radiation induced RMI, the inversion phase is delayed: we clearly observe a stagnation phase of the perturbation amplitude immediately following the velocity jump (Figure 6).

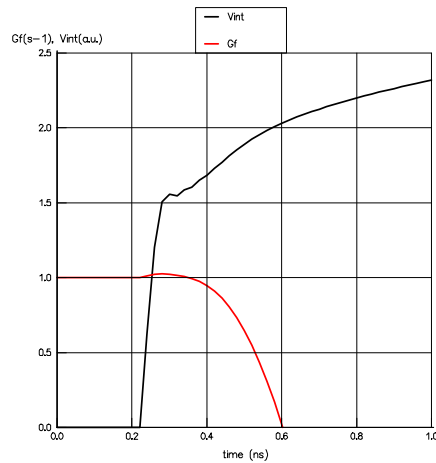


Figure 6: Growth factor and interface velocity time evolutions.

During the inversion phase of the interface perturbation the pressures in the heavy medium (Al) near the valleys of the perturbed interface, P_v , are necessarily greater than those near the peaks, P_p : see Figure 7.

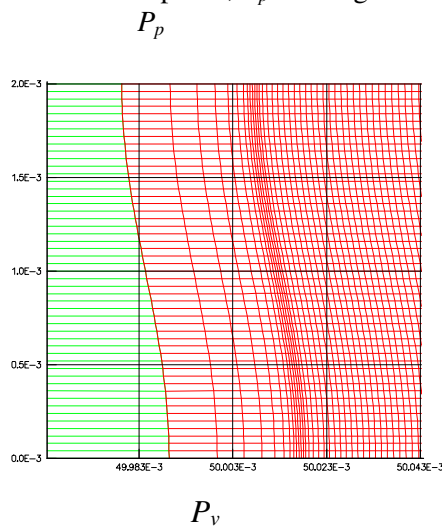


Figure 7: Locations of P_p and P_v .

For this reason the relative pressure perturbation, $\frac{\delta P}{P} \approx 2 \frac{P_p - P_v}{P_p + P_v}$, is negative during the inversion phase: see Figure 8. We also note that the relative temperature perturbation, $\frac{\delta T}{T}$, is very weak so that we have in fact $\frac{\delta P}{P} \approx \frac{\delta \rho}{\rho}$ (Figure 8).

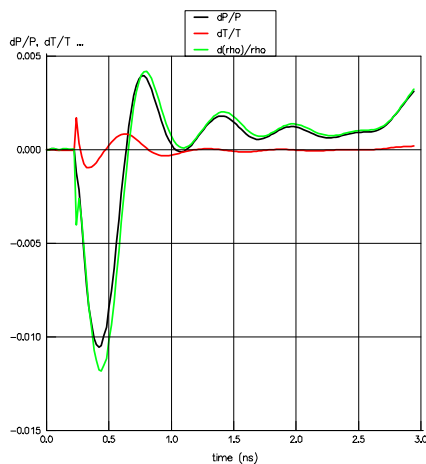


Figure 8: Time evolutions of the pressure, temperature and density relative perturbations on the Al side of the interface.

The inversion phase is thus directly related to the growth of the density in the valley regions which can only stem from a flow along the y -direction from peak to valley. Indeed the initial pressure of the heavy medium in the vicinity of the interface is y -independent because both the density and temperature ρ and T are y -independent. However the y -component of the velocity, V_y , is y -dependent due to the interface orientation (Figure 9).

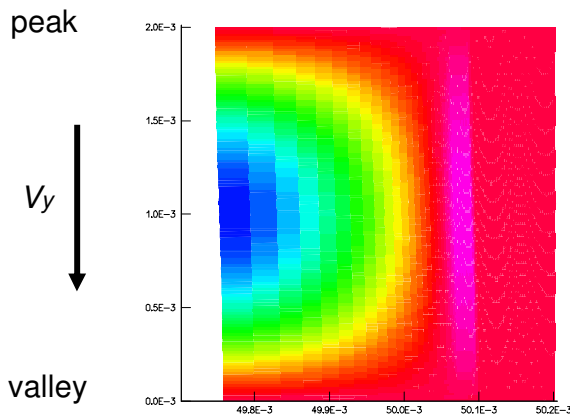


Figure 9: V_y map at the onset of the inversion phase.

The time evolutions of the velocity perturbation components δV_x and δV_y on the Al side of the interface shown in Figure 10 substantiate this interpretation. While δV_x has roughly a zero slope at the time of the velocity jump, corresponding to the stagnation phase, δV_y presents an initial jump which will generate the transverse density perturbation.

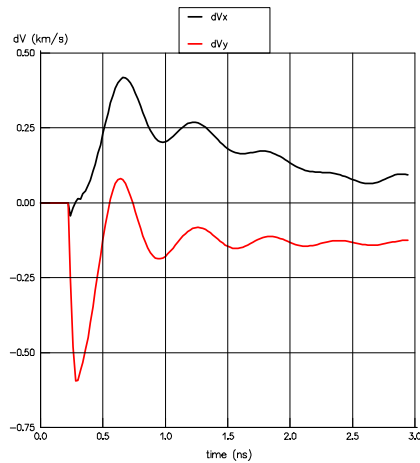


Figure 10: Time evolutions of the velocity perturbation components δV_x (black) and δV_y (red) on the interface Al side.

3- Multi-group diffusion

The preceding simulations were carried out with the Rosseland version of the FCI2 code (see “simulation methods”). Results obtained with the multi-group version of the FCI2 code are shown on Figure 11 which has to be compared with Figure 6 (Rosseland simulation):

Rosseland diffusion: all of the X-rays arrive at the same time on the interface, leading to a **single** velocity jump. The stagnation phase duration is 100 ps.

Multi-group diffusion: high energy X-rays generate a first velocity jump while low energy X-rays induce a secondary smoother jump of the interface velocity. Thus there are **two** velocity jumps and a longer stagnation phase (400 ps after the first velocity jump, the magnitude of which is half of the Rosseland simulation velocity jump).

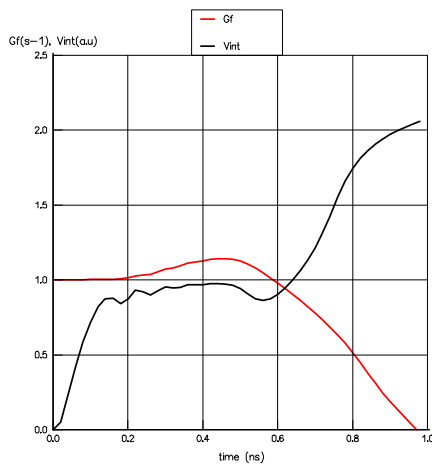


Figure 11: Growth factor and interface velocity time evolutions (multi-group diffusion).

SILEX simulations

SILEX is a 1D code solving the equations of gas dynamics with nonlinear heat conduction for both a planar-symmetric flow and its 3D linear perturbation transverse Fourier components (see [4] for more details). Nonlinear heat conduction is taken into account through a single power-law dependency of the heat conductivities in terms of fluid density and temperature, while different conductivity weights may be chosen for each material. For the system under

consideration, the density and temperature exponents of the heat conductivities were taken to be those of an analytical formula for the Rosseland mean free-path of Aluminum, while the conductivity weights of the CH foam and Aluminum were chosen to be roughly in the ratio 1 to 2000. Perfect gas equations of state were also used for both materials. Despite these simplifying assumptions, the simulation results are in all aspects very similar to those obtained with FCI2. In particular, a sharp rise of the interface mean velocity is obtained—although of magnitude smaller, by a factor of 2/3, than that of the FCI2 runs—, followed by a slowly decaying acceleration phase: see Figure 12. For a wavelength of 20 μm , the perturbation growth factor displays the same behavior (Figure 12) as that given by the equivalent FCI2 simulation (Figure 6). This resemblance between these two series of results strongly suggests that the basics of the present instability phenomena lie rather in the difference between the two material heat conductivities (or their optical thicknesses) than in the dependencies of the nonlinear conductivities (respectively mean free-paths) with respect to the density and temperature.

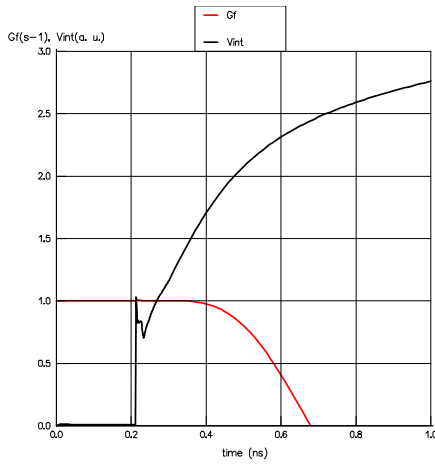


Figure 12: Growth factor and interface velocity time evolutions.

All perturbation computations were carried out with an initial grid point density, in the longitudinal direction, of at least 50 points per wavelength. In these simulations, thanks to the reduced computational cost of linear perturbation computations, we extended the range of perturbation wave-numbers investigated with 2D simulations by adding two smaller wavelengths: $\lambda = 5$ and $10 \mu\text{m}$. The growth factor results (Figure 13) present the same behaviors as those found with FCI2 simulations (Figure 3). In addition, growth factors for the two shortest wavelengths clearly exhibit phase reversals as well as damping of their time rate (Figure 14) in accordance with the slowly decaying acceleration phase experienced by the interface.

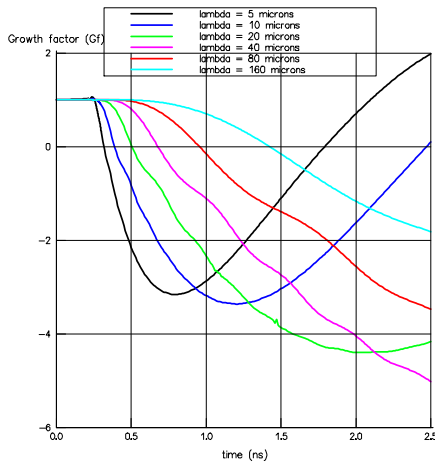


Figure 13: Growth factor of the instability (G_f).

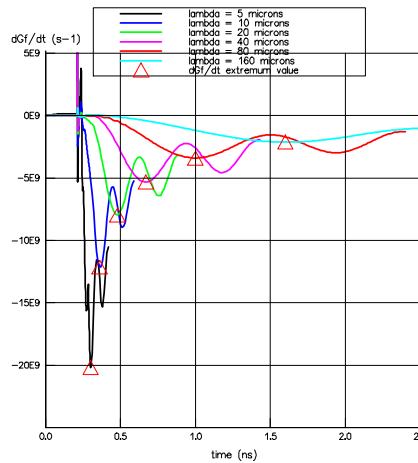


Figure 14: Growth factor time rate ($d(G_f)/dt$).

The linear regression of the extremal growth factor time rates, including the additional shorter wavelength data, shows a poorer agreement (Figure 15) than that observed with FIC2 results, thus confirming the limitations of such modeling.

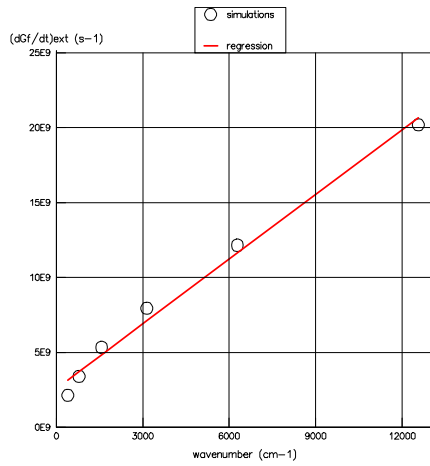


Figure 15: $(d(Gf)dt)_{ext}$ as a function of the wavenumber.

Finally, the graphs of the relative perturbation amplitudes for the temperature, density and pressure (Figure 16) as well as those for the x - and y -velocities (Figure 17) on the heavy (optically-thick) material side of the interface corroborate the preliminary analysis of the perturbation amplitude stagnation phase.

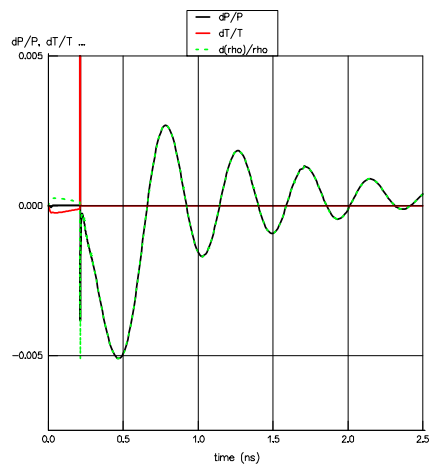


Figure 16: Time evolutions of the pressure, temperature and density relative perturbations on the Al side of the interface.

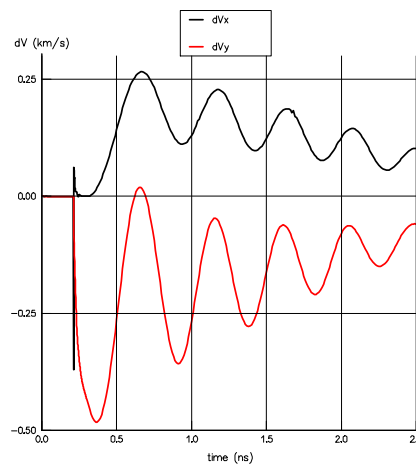


Figure 17: Time evolutions of the velocity perturbation components δV_x (black) and δV_y (red) on the interface Al side.

Summary

Base on careful numerical simulations, it appears that the radiation induced RMI considered in this study differs significantly from the classical RMI by two main features:

- a- The growth factor of the instability is not linearly time dependent.
- b- The perturbation amplitude stagnates for a significant duration immediately after the initial velocity jump.

However, after the stagnation phase the amplitude evolutions (inversion phase) can be described by an impulsive model for a short period of time.

The existence of this peculiar stagnation phase is directly related to the fact that the interface is impulsively set into motion under the sole action of the optically-thick material. While, following the velocity jump, no transverse gradients for the density, temperature, and therefore pressure, are initially present, a transverse velocity gradient immediately sets in (transverse velocity jump) which initiates the subsequent inversion phase. These findings are not qualitatively sensitive to the radiation model used (Rosseland or multi-group diffusion). Future work should lead to a theoretical modeling for this instability.

Acknowledgments

The authors would like to thank K.O. Mikaelian at LLNL who encouraged them to work in this very particular field and who shared with them many insights into hydrodynamic instability growth.

References

- [1] Mikaelian, K.O. Design calculations for a NOVA mix experiment; Proceedings of the 3rd IWPCTM, Royaumont, France, June 17-19, 1991, 137-144.
- [2] Goncharov, V.N. Theory of the ablative Richtmyer-Meshkov instability; Phys. Rev. Let. **82**, 2091 (1999).
- [3] Aglitskiy, Y. *et al.* Direct observation of mass oscillations due to ablative Richtmyer-Meshkov instability and feed out in planar plastic targets; Physics of plasmas **9**, 2264 (2002).
- [4] Boudesocque-Dubois, C. *et al.* this Workshop.